On the Role of the Flaming to Smoldering Transition in the Seasonal Cycle of African Fire Emissions

Bo Zheng, Frederic Chevallier, Philippe Ciais, Yi Yin, Yilong Wang

AGU100 ADVANCING EARTH AND SPACE SCIENCE

Geophysical Research Letters

RESEARCH LETTER
10.1029/2018GL079092

Key Points:
- CO emission factors of African fires likely rise up higher than the seasonally constant value used by GFED in the late fire season
- The increase in emission factors is partly due to a flaming to smoldering transition in relation with rainfall and fire radiative power
- The flaming to smoldering transition partly explains why the peak month in African fire emissions occurs later than GFED estimates

Supporting Information:
- Supporting Information S1
- Data Set S1

Correspondence to:
B. Zheng,
bo.zheng@lsce.ipsl.fr

Citation:
Zheng, B., Chevallier, F., Ciais, P., Yin, Y., & Wang, Y. (2018). On the role of the flaming to smoldering transition in the seasonal cycle of African fire emissions. *Geophysical Research Letters*, *45*, 11,998–12,007. https://doi.org/10.1029/2018GL079092

Received 5 JUN 2018
Accepted 22 OCT 2018
Accepted article online 25 OCT 2018
Published online 5 NOV 2018

On the Role of the Flaming to Smoldering Transition in the Seasonal Cycle of African Fire Emissions

Bo Zheng[1], Frederic Chevallier[1], Philippe Ciais[1], Yi Yin[1], and Yilong Wang[1]

[1]Laboratoire des Sciences du Climat et de l'Environnement, CEA-CNRS-UVSQ, UMR8212, Gif-sur-Yvette, France

Abstract Satellite estimates of burned area, associated carbon monoxide (CO) emission estimates, and CO column retrievals do not agree on the peak fire month in Africa, evident in both Northern and Southern Africa though distinct in the burning seasonality. Here we analyze this long-standing problem using (1) a top-down Bayesian inversion of Measurements Of Pollution In The Troposphere CO columns during 2005–2016 into surface CO emissions and (2) the bottom-up Global Fire Emissions Database 4.1 s. We show that Global Fire Emissions Database 4.1 s underestimates CO emissions by 12–62% in the late fire season and hypothesize that this is partly because it assumes seasonally static emission factors. However, the degree to which emission factors would have to vary through the season to bring top-down and bottom-up in agreement cannot be confirmed by past field-based measurements. Improved observational constraint on the seasonality of burned area, fuel combustion, and emission factors would further reduce the discrepancy between bottom-up and top-down emission estimates.

Plain Language Summary Fire is an integral component of African ecosystems, which emits large amounts of trace gases, pollutants, and aerosols into the atmosphere. The accurate assessment of this impact is currently hampered by the poor knowledge of fire emission estimates in Africa. One known issue is that the bottom-up estimates of carbon monoxide (CO) emissions using satellite-based burned area are generally underestimated and also describe a CO emission peak 1–2 months earlier than satellite CO column retrievals and their inversion into emissions. Here we used a Bayesian atmospheric inversion approach to analyze the seasonal variation in CO emissions, CO emission factors, and combustion efficiency of African savanna fires. The results lead us to hypothesize that under actual conditions, flaming- and smoldering-dominated combustions tend to appear successively when a moving fire front passes through a savanna. This mechanism is not sufficiently considered in current bottom-up fire emission models, which partly explains the emission underestimate and a phase shift to the early season in the seasonality of bottom-up emissions data.

1. Introduction

Fire is an integral component of many African ecosystems and especially of grasslands and savannas (Andela & van der Werf, 2014). The frequent and extensive fires in Africa emit large amounts of trace gases, pollutants, and aerosols into the atmosphere, which are an important research focus due to their significant influence on climate and air pollution. Among the emitted species, carbon monoxide (CO) has a lifetime of a few weeks, has no other major primary sources in Africa, and is observed by several satellite instruments. These features make CO a good tracer to study the African fires.

CO emission estimates for African fires are subject to considerable uncertainty, because the African fires are highly variable in space and time (Andela & van der Werf, 2014). Illustrative of those uncertainties, the top-down inversions of satellite CO column retrievals produce emission estimates 30% higher than bottom-up inventories in Africa (Chevallier et al., 2009; Liousse et al., 2010; Pétron et al., 2004; Stroppiana et al., 2010; Yin et al., 2015). Additionally, the top-down estimates (and CO columns from satellites) show a CO emission (and concentration) peak 1–2 months later than the bottom-up estimates (Roberts et al., 2009; Thonat et al., 2015; van der Werf et al., 2006; Whitburn et al., 2015). The fourth version of Global Fire Emissions Database (GFED 4.1 s) with improvements in the mapping of the burned area from small fires, and improved parameterizations of the conversion between burned area and burned fraction, has slightly improved the seasonal cycle of fire emissions in Africa (van der Werf et al., 2017), but it still cannot match the top-down inversions as discussed in this paper.

In this study, we analyze this problem from the perspective of the fire regime, with a focus on the seasonal variation of combustion efficiency and emission factors. The starting point is a Bayesian atmospheric inversion of tropospheric CO columns from Measurements Of Pollution In The Troposphere (MOPITT; Deeter et al., 2017) to estimate eight-daily maps of fire CO emissions between 2005 and 2016 (section 3). Then we use the inversion emissions and the GFED 4.1 s estimate of burned area (Giglio et al., 2013) and fuel combustion per unit area burned to calculate monthly CO emission factors (section 4). The estimated emission factors are compared to independent field measurement data and are then further used to deduce combustion efficiency at the monthly scale. Possible drivers of the seasonal variation in fire combustion efficiency are discussed in relation to terrestrial biomes, fire radiative power (FRP), and precipitation. These results lead us to discuss the evolving fire regime within a fire season and its influence on the seasonality of fire emissions (section 5). The logic of this research is summarized in Figure S1 in the supporting information.

2. Methods and Data

2.1. Inversion Analysis of CO Emissions

We use a Bayesian atmospheric inversion system (Chevallier et al., 2005) to infer eight-daily maps of CO emissions for years 2005–2016. Global CO emission fluxes are inferred from atmospheric observations of CO, formaldehyde (HCHO), and methane (CH_4) and from a priori emission maps, each information being weighted by its respective uncertainty. The a priori emissions of fires are derived from GFED 4.1 s, and the other input data are summarized in Figure S1 and Table S1 (Olivier et al., 2003; Granier et al., 2011; Sindelarova et al., 2014; González Abad et al., 2015). Detail of the current version of the inversion system is given by Zheng et al. (2018). Here we provide a brief summary.

The inversion system is built upon the Laboratoire de Météorologie Dynamique (LMDz)-Simplified Atmospheric Chemistry assimilation System (SACS) model (Pison et al., 2009), a 3-D transport model with a simplified chemistry scheme, and with an associated adjoint code. The chemical mechanism focuses on the hydrocarbon atmospheric oxidation chain, with explicit representation of CO, HCHO, CH_4, carbon dioxide (CO_2), and methyl chloroform (MCF). Observations of CO, HCHO, CH_4, and MCF are assimilated jointly into the inversion system. These observation data as well as a priori emissions are incorporated into a cost function (Text S1), which represents the misfit between simulation and observation, as well as the misfit between estimated and a priori emissions. The cost function is minimized using a quasi-Newton method in an iterative way to solve the inversion problem (Chevallier et al., 2005).

The inversion emissions of CO for all emitting sectors are solved for each surface grid cell of the LMDz-SACS model (1.9° latitude × 3.75° longitude) over 8-day periods (Yin et al., 2015). Fire emissions are then separated from total emissions in each grid cell by taking the product of optimized total emissions and the proportion of fire emissions derived from the a priori inventory (Yin et al., 2016). According to GFED 4.1 s and other a priori inventories (Table S1), fires account for more than 80% of CO emissions in the fire season over Africa. We calculate the monthly sum of fire emissions for the seasonal cycle analysis (Text S2).

2.2. Fire Emission Factor and Combustion Efficiency

We calculate monthly CO emission factors of African fires with the following formula:

$$EF_{i,j} = \frac{Emis_{i,j}}{BA_{i,j} \times Fuel_{i,j}} \tag{1}$$

where i represents the month during 2005–2016, j represents either Northern or Southern Africa (defined in Figure S2), *Emis* is inversion estimate of fire CO emissions (grams of CO), *BA* is the burned area (km^2) from GFED 4.1 s, *Fuel* is the fuel combustion per unit area burned (kilograms of dry matter per square kilometer) from GFED 4.1 s. The resulting emission factor *EF* is in grams of CO per kilogram of dry matter burned. We estimate the 95% confidence interval (CI) of *EF* by a Monte Carlo method, with the assumption of normal error statistics for *BA* and *Fuel* (Text S3). We assume that *BA* follows a normal distribution with a coefficient of variation (or *relative standard deviation*) of 10% (Giglio et al., 2010) and that the coefficient of variation for *Fuel* is 15% (van der Werf et al., 2017), both of which are independent of their quantities.

Modified combustion efficiency (MCE) is defined as the ratio of emitted carbon in CO_2 to emitted carbon in CO_2 + CO. This is an important indicator of burning efficiency, which estimates the relative share of flaming and smoldering combustion (Akagi et al., 2011). An MCE close to 1 reflects pure flaming and an MCE near 0.8 suggests mostly smoldering. Following van Leeuwen et al. (2013), we express the monthly MCE of African fires as a function of the CO emission factor:

$$MCE = a + b \times EF \tag{2}$$

We estimated the coefficients a and b as 1.0023 ± 0.0023 (95% CI) and −0.0009 ± 0.00003 (95% CI), respectively, on the basis of about 100 samples from different field measurements on savanna fires (Table S2). The R-squared value of this linear regression model is 0.98, a large value that gives us confidence in the robustness of this regression. Van Leeuwen et al. (2013) give similar estimates of a and b as 1.0041 and −0.0009, respectively. We also find that the negative linear relationship between MCE and emission factor holds for CH_4, particulate matters and ammonia (NH_3; Figure S3), which reflects the fact that fires emit more products of incomplete combustion at low combustion efficiency.

2.3. Driver Analysis of Combustion Efficiency

To investigate the drivers of the seasonal cycle of MCE, we empirically relate the estimated MCE to monthly FRP (Kaiser et al., 2012) and precipitation (CRU-NCEP version 7.2) using 2005–2016 average data (Figure S1 and Table S1). These two parameters are used as explaining variables because they are directly associated to fire characteristics. FRP represents fire radiative intensity (W/m^2), which is an indicator of fire energy (Tang & Arellano, 2017; Wooster et al., 2005) and of biomass combustion (Kaiser et al., 2012). Precipitation shapes fire regimes through limiting burned area and altering fuel moisture content. We also combine land cover maps with burned area to check if a shift from grassland fires to woodland fires occurs in the late fire season. This is a widely cited conjecture to explain the mismatch in seasonality of fire CO emissions between bottom-up and top-down estimates (van der Werf et al., 2006). We use two independent land cover maps from Li et al. (2018) and Hansen et al. (2013) for comparison, and we also use two different burned area products from GFED 4.1 s and MERIS 4.1 (Pettinari et al., 2016), respectively.

3. Annual Patterns and Seasonal Variations of African Fire CO Emissions

The largest burned area in Africa (Figure S2) is observed in savanna with available biomass as fuel load during the dry season when fire occurs. The fire season typically starts from Northern Africa in October, moves southward and ends near the southeast coast of Southern Africa by October on the following year. The most widespread fire with maximum burned area generally occurs in December and January over Northern Africa, and in July and August over Southern Africa. After those months, the burned area starts to decrease, and Africa enters the late fire season.

The inversion-estimated fire CO emissions are significantly higher than the a priori field from GFED 4.1 s (Figures 1a and 1b). The lower values of GFED 4.1 s are evident over the whole continent of Africa, that is, −12% to −55% in Northern Africa from January to March (Figure 1c) and −31% to −62% in Southern Africa from August to October (Figure 1d), which suggests that GFED gives lower estimates of emissions in the late fire season. The seasonal variation in GFED emissions is broadly consistent with the FRP-derived emissions from Global Fire Assimilation System (GFAS) version 1.2 (Figures 1c and 1d). To represent fire emissions, GFED uses satellite-based burned area (van der Werf et al., 2017), while GFAS uses satellite-based FRP (Kaiser et al., 2012). Despite different proxies, the temporal variation in total carbon emissions are consistent between GFED and GFAS. Both GFED and GFAS use seasonally static emission factors to calculate CO emissions from total carbon release; therefore, the seasonal variation of their CO emissions follow each other.

Modeling results of LMDz-SACS of CO columns driven by GFED 4.1 s agree with MOPITT CO columns in the early months of a fire season but underestimate the CO columns during the late season (Figure S4). The underestimation of CO columns exceeds the interannual variation in MOPITT observations, a feature that was also seen in other studies that used different atmospheric transport models and previous versions of the GFED data (Edwards et al., 2006; van Leeuwen et al., 2013). Additionally, the models driven by GFED cannot reproduce the late peak of satellite retrievals of NH_3 columns (Paulot et al., 2017) and aerosol optical depth (AOD; Horowitz et al., 2017; Magi et al., 2009; Tummon et al., 2010) over Africa. These tracers follow different chemical

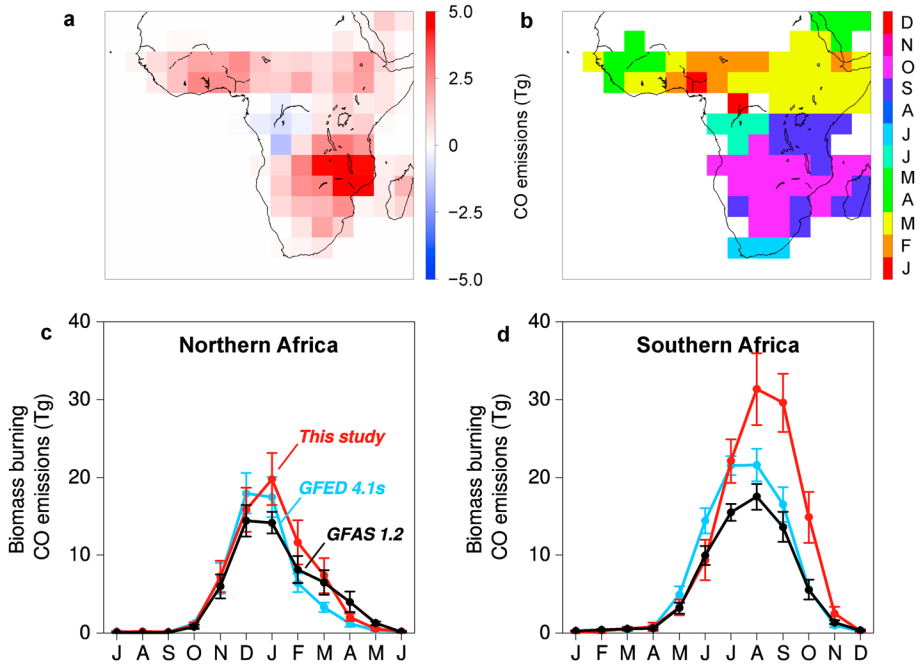

Figure 1. Inverse analysis of African fire CO emissions. The differences of average annual fire CO emissions between inversion and GFED 4.1 s (i.e., inversion emissions minus GFED 4.1 s) are shown in (a), and the months when the largest differences occur are shown in (b). Both (a) and (b) are mapped at 5° × 5°. Average monthly fire CO emissions are calculated using GFED 4.1 s (blue curve), GFAS 1.2 (black curve), and the inversion emissions (red curve) in (c) and (d), and plotted with error bars that represent one standard deviation induced by the interannual variation of 2005–2016 data. Note that the *x*-axis of (c) is ordered from July to June. GFAS = Global Fire Assimilation System; GFED = Global Fire Emissions Database.

processes than CO and have shorter atmospheric lifetimes; therefore, the modeling biases are probably caused by the underestimated emissions of GFED in the late season rather than by modeling deficiencies.

Compared to bottom-up emission estimates, the late peak of the inversion emissions has also been observed by studies that assimilated previous releases of MOPITT or Infrared Atmospheric Sounding Interferometer (IASI) retrievals in different data assimilation systems (Arellano et al., 2006; Chevallier et al., 2009; Pétron et al., 2004; Whitburn et al., 2015). We interpret the consistency with other inversion studies as a sign of robustness of the delayed timing in CO emissions retrieved in this study, when compared to both GFED and GFAS.

4. Seasonal Variation of CO Emission Factor, Combustion Efficiency, and Their Drivers

The inversion emissions combined with equations (1) and (2) suggest a seasonal variation in CO emission factor and MCE, unlike the seasonally constant values assumed in GFED 4.1 s (Figure 2). The estimated CO emission factors remain close to the GFED value (i.e., 63 g/kg dry matter) in the early season but increase rapidly in the late season. These variations suggest that MCE remains constant at 0.94–0.96 at the beginning of a fire season, that is, October–December for Northern Africa (Figure 2d) and May–July for Southern Africa (Figure 2e) then decreases linearly to 0.84–0.87 during the following 3 months. Compared to independent field measurement data (Figure 2a), the seasonal variation in the estimated MCE (and emission factors) are mainly within 1-sigma of the average measured data (Figures 2b–2e), except the minimum MCE (and maximum emission factors) present in March for Northern Africa and in October and November for Southern Africa.

Declining trends in combustion efficiency during the late fire season appear to be consistent with satellite measurement of fire characteristics. Mebust and Cohen (2013) estimated NO_x emission factors for wildfires using Ozone Monitoring Instrument (OMI) nitrogen dioxide (NO_2) satellite retrievals (without any

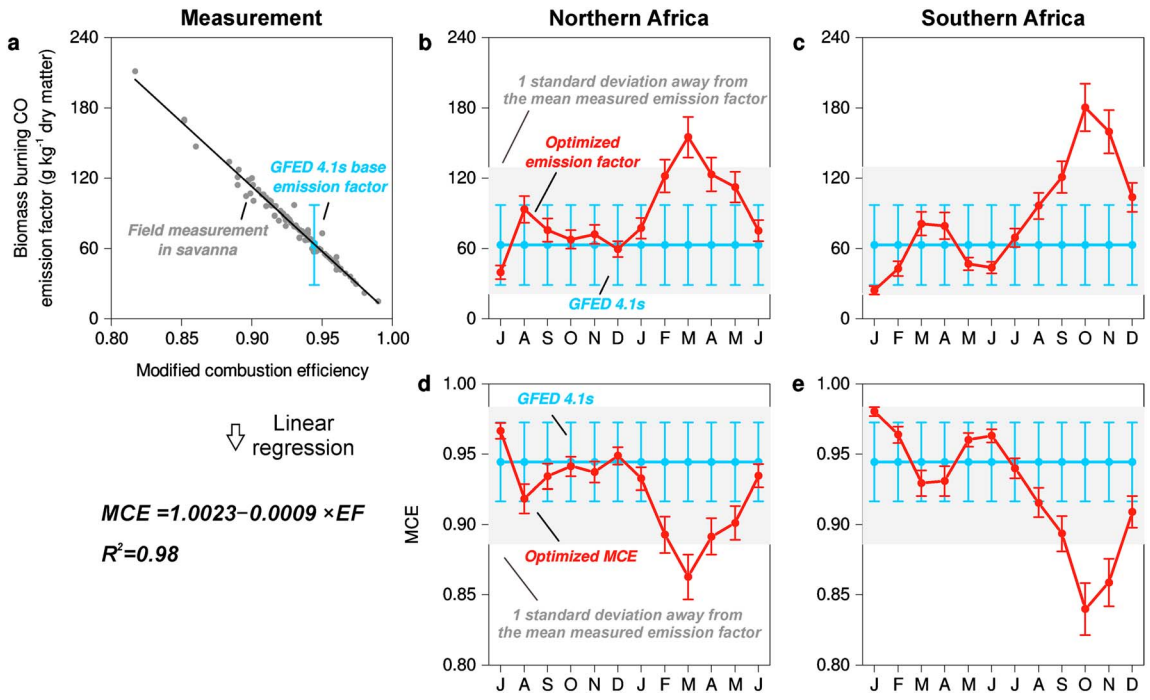

Figure 2. Seasonal variation in CO emission factors and MCE of African savanna fires. The gray disks in (a) are the field measurement data that we use to build the linear regression model of MCE (*x*-axis) and CO emission factors (*y*-axis). These data are summarized in Table S2 (Desservettaz et al., 2017; Sinha et al., 2003; Smith et al., 2014; Ward et al., 1996; Wooster et al., 2011; Yokelson et al., 2003; Yokelson et al., 2011). The blue dot in (a) is the emission factor used by the GFED 4.1 s database. Average monthly emission factors and MCE from the inversion estimates are plotted for Northern Africa (red disks in (b) and (d)) and Southern Africa (red disks in (c) and (e)), respectively. The GFED seasonally static emission factors are plotted as blue circles in (b)–(e). The error bars in (a)–(e) represent a 95% confidence interval (CI). The 95% CI of the inversion results are estimated by a Monte Carlo method (Text S3). The 95% CI of the GFED data are from van der Werf et al. (2017). Note that the *x*-axis in (b) and (d) is ordered from July to June. GFED = Global Fire Emissions Database; MCE = modified combustion efficiency.

chemistry-transport model in contrast to here, thanks to the short lifetime of NO_2) and found them decreasing in January–March over Northern Africa and in August–October over Southern Africa. Castellanos et al. (2014) used OMI NO_2 data to study Southern American fires and also identified a similar decrease in NO_x emission factors of savanna fires in the late season. Since NO_x is more efficiently produced at high MCE, the decrease of NO_x emission factors could suggest a decrease in MCE during the late fire season, although we cannot rule out the influence from the declining nitrogen content in grasses as they senesce (Mebust & Cohen, 2013). Tang and Arellano (2017) also observed an overall decrease in combustion efficiency across the fire season in the Amazon basin (with more forest fires than Africa) based on multiple satellite data sets. Despite the possible agreement, the magnitudes of MCE estimated in our study still remain uncertain. The maximum *EF* estimated in the late fire season (Figures 2b–2e) falls outside the 1-sigma range of the average measured local field data (displayed in gray in the figure). Few measurement data therefore reach this estimated maximum: we may wonder whether such large values can really persist for a whole month or whether they are overestimated.

By definition (from equation (1)), the larger *EF* inferred from the CO inversion fluxes could be explained by higher *Emis*, lower *BA*, or lower *Fuel*. *Emis* is constrained by multispecies observations and is consistent with many other studies as discussed in section 3. For *BA* and *Fuel*, both derived from GFED 4.1 s, we observe that they rapidly decline during the late season. *BA* and *Fuel* decrease by 68% and 19%, respectively, from August to October over Southern Africa. During the same period, the inversion CO emissions decrease by 53% and the resulting *EF* increase by 87%. The sharp decrease in *BA* and *Fuel* must therefore be the primary explanation for the inversion-derived *EF*s higher than the GFED 4.1 s ones. Despite the inclusion of small fires in GFED 4.1 s compared to GFED 4 (mainly in the early fire season, see Figure S8), GFED 4.1 s may still miss small fires in the late season and therefore may overestimate the decline in *BA*. Seasonal variations of the parameter *Fuel* are constrained by few observations. Airborne measurements typically focus on extensive fires (Hoffa et al., 1999; Korontzi et al., 2003) without smoldering combustion (Andreae & Merlet, 2001). Given the large

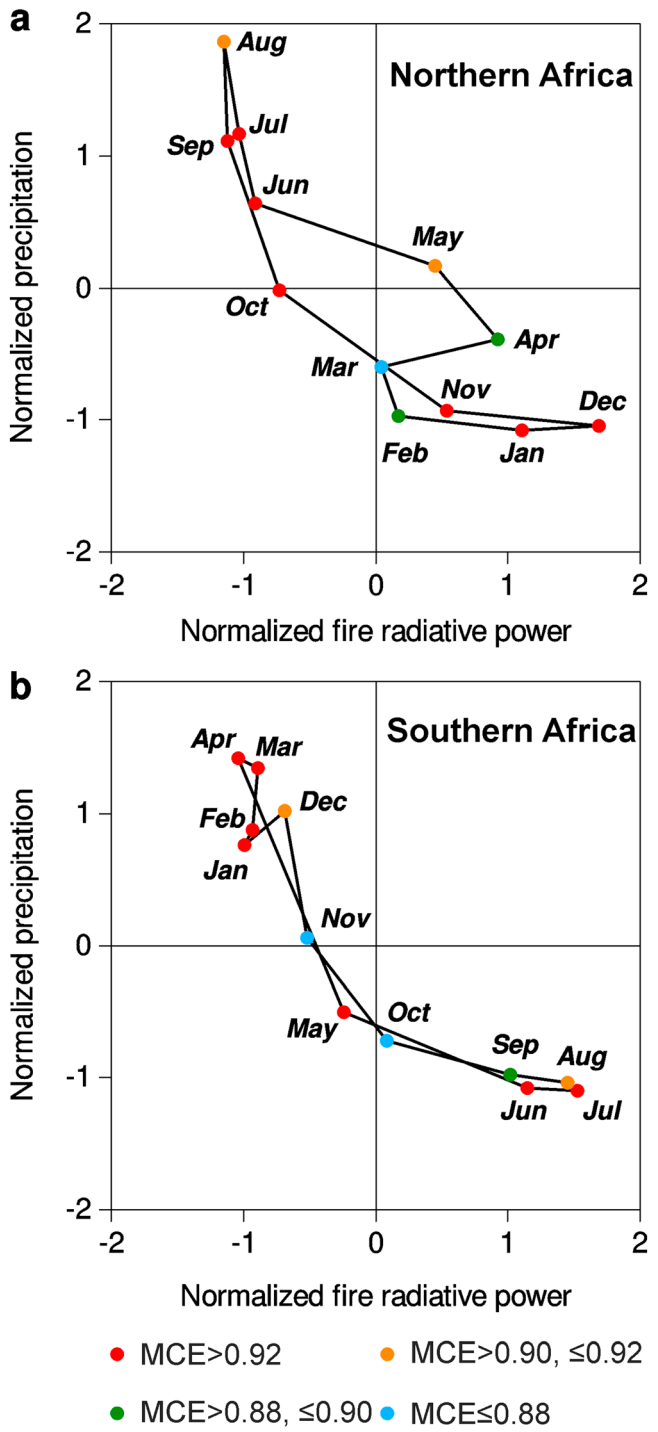

Figure 3. Evolution of MCE with fire radiative power and precipitation over Northern Africa (a) and Southern Africa (b). We first estimate the seasonal variation of fire radiative power (spatial average) and precipitation (burned area weighted average) with 2005–2016 data (Text S2). Then each month is plotted according to its fire radiative power (*x*-axis) and precipitation (*y*-axis) with the color representing the monthly average MCE. MCE = modified combustion efficiency.

variation in the measured *EF* due to distinct MCE (Figure 2), using an emission factor averaged from sample measurements is subject to potentially large uncertainty, and does not well represent fire dynamics. We obviously need more field measurements to inform equation (1).

Figure 3 analyzes the drivers of seasonal variations in combustion efficiency. In a fire season cycle, the early season with a high MCE (>0.92) is accompanied by increasing FRP and decreasing precipitation, while the late season sees an opposite trend, that is, lower FRP and higher precipitation that produce low MCE. These results suggest that FRP and precipitation can be used to describe the seasonal cycle of MCE, probably because fire temperatures and fuel moisture content are the main drivers of combustion efficiency. In contrast to Africa, the late dry season in Australian savanna is accompanied by little rain and hot dry winds and does not induce significant seasonality in fire emission factors (Meyer et al., 2012).

Another possible driver of MCE is the fuel structure (Meyer et al., 2012; Meyer & Cook, 2015), or the ratio of grassland fires to woodland fires. The coarse woody biomass (e.g., stems and woody debris) that have low surface-area-to-volume ratios cannot burn fast and release heat efficiently, thus contribute to a low MCE (Urbanski, 2013) and to more CO emissions per unit carbon burned. van der Werf et al. (2006) speculated that the increasing CO emissions in the late fire season over Africa were probably caused by the shift from grassland fires to woodland fires. This view, although not yet fully validated, has been widely cited in the literature. Here we make an attempt to overlay monthly burned area with land cover maps to confirm this conjecture, but we detect fewer woody land cover affected by burning in the late season than in the early season (Figure S5). This is evident and robust to different burned area and land cover maps. Despite such results, we still cannot falsify the point made by van der Werf et al. (2006) due to the uncertainties of this analysis. The spatial resolution of burned area and land cover maps is of several hundred meters, so the fine-scale fire dynamics at the resolution of tens of meters may not be captured. Land cover maps also have a large uncertainty (e.g., positional and categorical) at fine scales. High-resolution data may help to justify the role of fuel structure that plays in the seasonal variation of emission factors and MCE.

5. Revisiting the Mismatch Between Top-Down and Bottom-Up Emission Estimates

The seasonal variation in MCE is consistent with a transition from flaming-dominated to smoldering-dominated fires in the late season. The flaming combustion that typically occurs at ~1,400 K involves thermal cracking of biomass, formation of flammable volatile compounds, and rapid oxidation into highly oxidized gases (e.g., NO_x and CO_2). Smoldering combustion mainly involves gas-solid reaction at fuel surface (i.e., surface oxidation), which produces incompletely oxidized pyrolysis products at 800–1,000 K, such as CO, CH_4, NH_3, and organic aerosols. The flaming to smoldering transition should drive up CO emissions in the late season and explain some of the 1- to 2-month delayed peak in inversion CO emissions compared to GFED 4.1 s. We cannot explain all of this delay because we may overestimate the true increase in emission factors in the late season. We likely need more observations to constrain the seasonal variations of

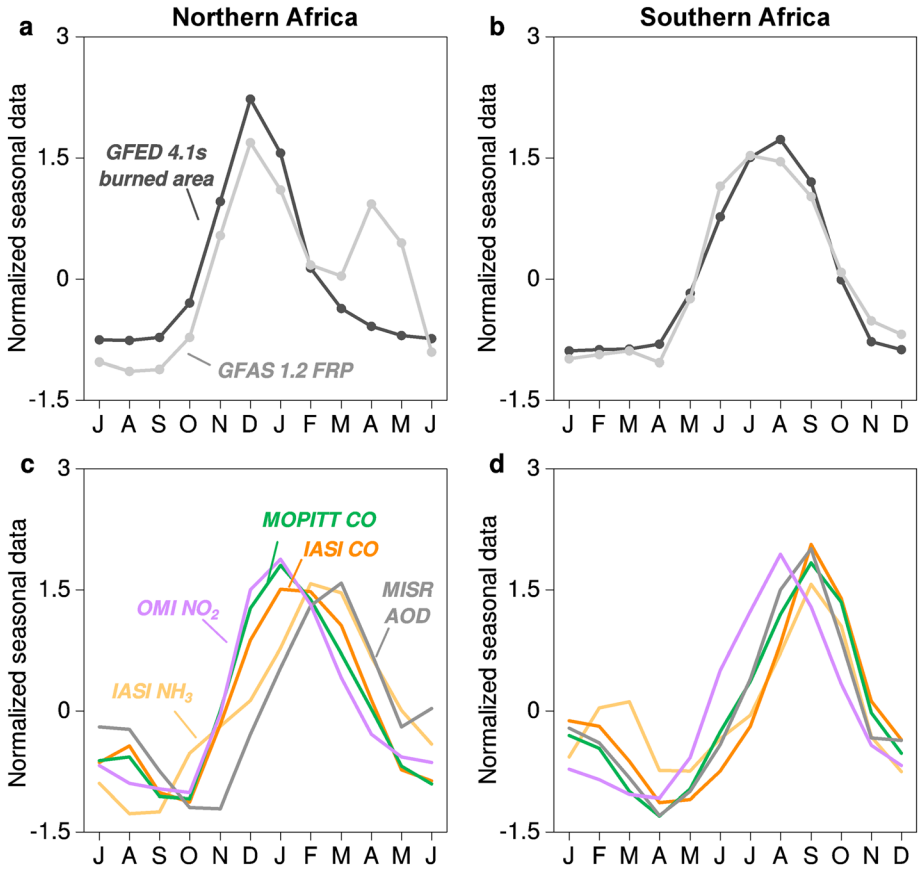

Figure 4. Seasonal variation of burned area and pyrogenic species concentrations observed by satellite over Northern Africa (a and c) and Southern Africa (b and d). The normalized seasonal data are estimated using the curve fitting method as described in Text S2. GFED = Global Fire Emissions Database; GFAS = Global Fire Assimilation System; MISR = Multiangle Imaging SpectroRadiome; AOD = aerosol optical depth; IASI = Infrared Atmospheric Sounding Interferometer; OMI = Ozone Monitoring Instrument; MOPITT = Measurements Of Pollution In The Troposphere.

burned area, fuel combustion, and emission factors. Ground-based air sampling of fresh smoke plumes are currently biased towards the flaming combustion and often miss the smoldering combustion with low MCE that can occur over periods of days to weeks after the fire passage. For instance, of the 55 measurement data over Southern Africa (Table S2), 42 samples were measured during June–August, while only 13 samples were for September.

As mentioned in section 3, the mismatch in seasonality of CO emissions is also evident for other pyrolysis species over Africa. Figures 4c and 4d show satellite column retrievals of CO, NH_3, NO_2, and AOD over Africa. The columns of CO from MOPITT (Deeter et al., 2017) and IASI (George et al., 2015), NH_3 from IASI (Van Damme et al., 2017), and AOD from Multiangle Imaging SpectroRadiome (Multiangle Imaging SpectroRadiome Science Team, 2015) follow each other well and all peak 1–2 months later than burned area and FRP. These species are primarily emitted by fires (CO as an example in Figure S6) and corresponding satellite retrievals represent an integral of gases of a range of ages from fresh smoke plumes through to aged smoke. According to field measurements (Table S2 and Figure S3), fire emission factors of CH_4, NH_3, and particulate matter increase linearly with MCE decreasing. As MCE decreases during the late season, fires emit more CH_4, NH_3, and aerosols per unit of area burned. This could partly explain the mismatch in seasonal variations between burned area and satellite observed column concentrations. The OMI NO_2 columns (Boersma et al., 2011) are broadly consistent with the seasonal cycle of burned area and FRP, because NO_2 is mainly produced from flaming fires, and the smoldering combustion in the late season does not increase its emission factor. All the features discussed above remain robust during 2005–2016 on the basis of decadal time series of data analyzed in Figure 4.

6. Conclusions

We analyzed the mismatch in African fire emissions between top-down and bottom-up estimates using Bayesian atmospheric inversion and independent related data sets. The results lead us to hypothesize that emission factors of CO (and of other incompletely oxidized species) tend to be increased by rising precipitation and declining FRP during the flaming to smoldering transition in the late fire season, which would partly explain the 1–2 month delayed peak in inversion fire emissions compared to GFED 4.1 s (and GFAS 1.2). This mechanism alone may not bring top-down and bottom-up estimates in total agreement, because we may overestimate the true increase in emission factors in the late season, for instance through imperfect knowledge of the seasonality of burned area and fuel combustion. More high-resolution observations (in particular for smoldering combustion with low MCE) are needed to further improve the understanding of African fire emissions.

Acknowledgments
Data to support this research are available in the supporting information. We acknowledge the data providers of NCAR MOPITT for satellite CO retrievals, SAO OMI for CH_2O retrievals, and WDCGG for CH_4, CO, and MCF surface air-sample measurements. We also thank F. Marabelle for computer support at LSCE. The present work was also granted access to the HPC resources of TGCC under allocation A0030102201.

References

Akagi, S. K., Yokelson, R. J., Wiedinmyer, C., Alvarado, M. J., Reid, J. S., Karl, T., Crounse, J. D., et al. (2011). Emission factors for open and domestic biomass burning for use in atmospheric models. *Atmospheric Chemistry and Physics*, *11*(9), 4039–4072. https://doi.org/10.5194/acp-11-4039-2011

Andela, N., & van der Werf, G. R. (2014). Recent trends in African fires driven by cropland expansion and El Niño to La Niña transition. *Nature Climate Change*, *4*(9), 791–795. https://doi.org/10.1038/nclimate2313

Andreae, M. O., & Merlet, P. (2001). Emission of trace gases and aerosols from biomass burning. *Global Biogeochemical Cycles*, *15*(4), 955–966. https://doi.org/10.1029/2000GB001382

Arellano, A. F., Kasibhatla, P. S., Giglio, L., van der Werf, G. R., Randerson, J. T., & Collatz, G. J. (2006). Time-dependent inversion estimates of global biomass-burning CO emissions using measurement of pollution in the troposphere (MOPITT) measurements. *Journal of Geophysical Research*, *111*, D09303. https://doi.org/10.1029/2005JD006613

Boersma, K. F., Eskes, H. J., Dirksen, R. J., van der A, R. J., Veefkind, J. P., Stammes, P., Huijnen, V., et al. (2011). An improved tropospheric NO_2 column retrieval algorithm for the Ozone Monitoring Instrument. *Atmospheric Measurement Techniques*, *4*(9), 1905–1928. https://doi.org/10.5194/amt-4-1905-2011

Castellanos, P., Boersma, K. F., & van der Werf, G. R. (2014). Satellite observations indicate substantial spatiotemporal variability in biomass burning NO_x emission factors for South America. *Atmospheric Chemistry and Physics*, *14*(8), 3929–3943. https://doi.org/10.5194/acp-14-3929-2014

Chevallier, F., Fisher, M., Peylin, P., Serrar, S., Bousquet, P., Bréon, F. M., Chédin, A., et al. (2005). Inferring CO_2 sources and sinks from satellite observations: Method and application to TOVS data. *Journal of Geophysical Research*, *110*, D24309. https://doi.org/10.1029/2005JD006390

Chevallier, F., Fortems, A., Bousquet, P., Pison, I., Szopa, S., Devaux, M., & Hauglustaine, D. A. (2009). African CO emissions between years 2000 and 2006 as estimated from MOPITT observations. *Biogeosciences*, *6*(1), 103–111. https://doi.org/10.5194/bg-6-103-2009

Deeter, M. N., Edwards, D. P., Francis, G. L., Gille, J. C., Martínez-Alonso, S., Worden, H. M., & Sweeney, C. (2017). A climate-scale satellite record for carbon monoxide: The MOPITT version 7 product. *Atmospheric Measurement Techniques*, *10*(7), 2533–2555. https://doi.org/10.5194/amt-10-2533-2017

Desservettaz, M., Paton-Walsh, C., Griffith, D. W. T., Kettlewell, G., Keywood, M. D., Vanderschoot, M. V., Ward, J., et al. (2017). Emission factors of trace gases and particles from tropical savanna fires in Australia. *Journal of Geophysical Research: Atmospheres*, *122*, 6059–6074. https://doi.org/10.1002/2016JD025925

Edwards, D. P., Emmons, L. K., Gille, J. C., Chu, A., Attié, J. L., Giglio, L., Wood, S. W., et al. (2006). Satellite-observed pollution from Southern Hemisphere biomass burning. *Journal of Geophysical Research*, *111*, D14312. https://doi.org/10.1029/2005JD006655

George, M., Clerbaux, C., Bouarar, I., Coheur, P. F., Deeter, M. N., Edwards, D. P., Francis, G., et al. (2015). An examination of the long-term CO records from MOPITT and IASI: Comparison of retrieval methodology. *Atmospheric Measurement Techniques*, *8*(10), 4313–4328. https://doi.org/10.5194/amt-8-4313-2015

Giglio, L., Randerson, J. T., & van der Werf, G. R. (2013). Analysis of daily, monthly, and annual burned area using the fourth-generation Global Fire Emissions Database (GFED4). *Journal of Geophysical Research: Biogeosciences*, *118*, 317–328. https://doi.org/10.1002/jgrg.20042

Giglio, L., Randerson, J. T., van der Werf, G. R., Kasibhatla, P. S., Collatz, G. J., Morton, D. C., & DeFries, R. S. (2010). Assessing variability and long-term trends in burned area by merging multiple satellite fire products. *Biogeosciences*, *7*(3), 1171–1186. https://doi.org/10.5194/bg-7-1171-2010

González Abad, G., Liu, X., Chance, K., Wang, H., Kurosu, T. P., & Suleiman, R. (2015). Updated Smithsonian Astrophysical Observatory Ozone Monitoring Instrument (SAO OMI) formaldehyde retrieval. *Atmospheric Measurement Techniques*, *8*(1), 19–32. https://doi.org/10.5194/amt-8-19-2015

Granier, C., Bessagnet, B., Bond, T., D'Angiola, A., Denier van der Gon, H., Frost, G. J., Heil, A., et al. (2011). Evolution of anthropogenic and biomass burning emissions of air pollutants at global and regional scales during the 1980–2010 period. *Climatic Change*, *109*(1-2), 163–190. https://doi.org/10.1007/s10584-011-0154-1

Hansen, M. C., Potapov, P. V., Moore, R., Hancher, M., Turubanova, S. A., Tyukavina, A., Thau, D., et al. (2013). High-resolution global maps of 21st-century forest cover change. *Science*, *342*(6160), 850–853. https://doi.org/10.1126/science.1244693

Hoffa, E. A., Ward, D. E., Hao, W. M., Susott, R. A., & Wakimoto, R. H. (1999). Seasonality of carbon emissions from biomass burning in a Zambian savanna. *Journal of Geophysical Research*, *104*(D11), 13,841–13,853. https://doi.org/10.1029/1999JD900091

Horowitz, H. M., Garland, R. M., Thatcher, M., Landman, W. A., Dedekind, Z., van der Merwe, J., & Engelbrecht, F. A. (2017). Evaluation of climate model aerosol seasonal and spatial variability over Africa using AERONET. *Atmospheric Chemistry and Physics*, *17*(22), 13,999–14,023. https://doi.org/10.5194/acp-17-13999-2017

Kaiser, J. W., Heil, A., Andreae, M. O., Benedetti, A., Chubarova, N., Jones, L., Morcrette, J. J., et al. (2012). Biomass burning emissions estimated with a Global Fire Assimilation System based on observed fire radiative power. *Biogeosciences*, *9*(1), 527–554. https://doi.org/10.5194/bg-9-527-2012

Korontzi, S., Ward, D. E., Susott, R. A., Yokelson, R. J., Justice, C. O., Hobbs, P. V., Smithwick, E. A. H., et al. (2003). Seasonal variation and ecosystem dependence of emission factors for selected trace gases and PM2.5 for southern African savanna fires. *Journal of Geophysical Research*, *108*(D24), 4758. https://doi.org/10.1029/2003JD003730

Li, W., MacBean, N., Ciais, P., Defourny, P., Lamarche, C., Bontemps, S., Houghton, R. A., et al. (2018). Gross and net land cover changes in the main plant functional types derived from the annual ESA CCI land cover maps (1992–2015). *Earth System Science Data*, *10*(1), 219–234. https://doi.org/10.5194/essd-10-219-2018

Liousse, C., Guillaume, B., Grégoire, J. M., Mallet, M., Galy, C., Pont, V., Akpo, A., et al. (2010). Updated African biomass burning emission inventories in the framework of the AMMA-IDAF program, with an evaluation of combustion aerosols. *Atmospheric Chemistry and Physics*, *10*(19), 9631–9646. https://doi.org/10.5194/acp-10-9631-2010

Magi, B. I., Ginoux, P., Ming, Y., & Ramaswamy, V. (2009). Evaluation of tropical and extratropical Southern Hemisphere African aerosol properties simulated by a climate model. *Journal of Geophysical Research*, *114*, D14204. https://doi.org/10.1029/2008JD011128

Mebust, A. K., & Cohen, R. C. (2013). Observations of a seasonal cycle in NOx emissions from fires in African woody savannas. *Geophysical Research Letters*, *40*, 1451–1455. https://doi.org/10.1002/grl.50343

Meyer, C. P., & Cook, G. D. (2015). Biomass combustion and emission processes in the northern Australian savannas. In B. P. Murphy, A. C. Edwards, M. Meyer, & J. Russell-Smith (Eds.), *Carbon accounting and savanna fire management* (Chap. 9, pp. 185–217). Melbourne: CSIRO Publishing.

Meyer, C. P., Cook, G. D., Reisen, F., Smith, T. E. L., Tattaris, M., Russell-Smith, J., Maier, S. W., et al. (2012). Direct measurements of the seasonality of emission factors from savanna fires in northern Australia. *Journal of Geophysical Research*, *117*, D20305. https://doi.org/10.1029/2012JD017671

Olivier J., Peters, J., Granier, C., Petron, G., Muller, J. F., & Wallens, S. (2003). Present and future surface emissions of atmospheric compounds, POET report #2, EU project EVK2–1999-00011.

Paulot, F., Paynter, D., Ginoux, P., Naik, V., Whitburn, S., Van Damme, M., Clarisse, L., et al. (2017). Gas-aerosol partitioning of ammonia in biomass burning plumes: Implications for the interpretation of spaceborne observations of ammonia and the radiative forcing of ammonium nitrate. *Geophysical Research Letters*, *44*, 8084–8093. https://doi.org/10.1002/2017GL074215

Pétron, G., Granier, C., Khattatov, B., Yudin, V., Lamarque, J.-F., Emmons, L., Gille, J., et al. (2004). Monthly CO surface sources inventory based on the 2000–2001 MOPITT satellite data. *Geophysical Research Letters*, *31*, L21107. https://doi.org/10.1029/2004GL020560

Pettinari, M. L., Chuvieco, E., Alonso-Canas, I., Storm, T., & Padilla Parellada, M. (2016). ESA CCI ECV fire disturbance: Product user guide, version 2.1. Retrieved from http://www.esa-fire-cci.org/documents

Pison, I., Bousquet, P., Chevallier, F., Szopa, S., & Hauglustaine, D. (2009). Multi-species inversion of CH_4, CO and H_2 emissions from surface measurements. *Atmospheric Chemistry and Physics*, *9*(14), 5281–5297. https://doi.org/10.5194/acp-9-5281-2009

Roberts, G., Wooster, M. J., & Lagoudakis, E. (2009). Annual and diurnal african biomass burning temporal dynamics. *Biogeosciences*, *6*(5), 849–866. https://doi.org/10.5194/bg-6-849-2009

Science Team, M. I. S. R. (2015). *Terra/MISR level 3, component global aerosol monthly, version 4*. Hampton, VA, USA: NASA Atmospheric Science Data Center (ASDC). https://doi.org/10.5067/Terra/MISR/MIL3MAE_L3.004

Sindelarova, K., Granier, C., Bouarar, I., Guenther, A., Tilmes, S., Stavrakou, T., Müller, J. F., et al. (2014). Global data set of biogenic VOC emissions calculated by the MEGAN model over the last 30 years. *Atmospheric Chemistry and Physics*, *14*(17), 9317–9341. https://doi.org/10.5194/acp-14-9317-2014

Sinha, P., Hobbs, P. V., Yokelson, R. J., Bertschi, I. T., Blake, D. R., Simpson, I. J., Gao, S., et al. (2003). Emissions of trace gases and particles from savanna fires in southern Africa. *Journal of Geophysical Research*, *108*(D13), 8478. https://doi.org/10.1029/2002JD002325

Smith, T. E. L., Paton-Walsh, C., Meyer, C. P., Cook, G. D., Maier, S. W., Russell-Smith, J., Wooster, M. J., et al. (2014). New emission factors for Australian vegetation fires measured using open-path Fourier transform infrared spectroscopy—Part 2: Australian tropical savanna fires. *Atmospheric Chemistry and Physics*, *14*(20), 11,335–11,352. https://doi.org/10.5194/acp-14-11335-2014

Stroppiana, D., Brivio, P. A., Grégoire, J. M., Liousse, C., Guillaume, B., Granier, C., Mieville, A., et al. (2010). Comparison of global inventories of CO emissions from biomass burning derived from remotely sensed data. *Atmospheric Chemistry and Physics*, *10*(24), 12,173–12,189. https://doi.org/10.5194/acp-10-12173-2010

Tang, W., & Arellano, A. F. Jr. (2017). Investigating dominant characteristics of fires across the Amazon during 2005–2014 through satellite data synthesis of combustion signatures. *Journal of Geophysical Research: Atmospheres*, *122*, 1224–1245. https://doi.org/10.1002/2016JD025216

Thonat, T., Crevoisier, C., Scott, N. A., Chédin, A., Armante, R., & Crépeau, L. (2015). Signature of tropical fires in the diurnal cycle of tropospheric CO as seen from Metop-A/IASI. *Atmospheric Chemistry and Physics*, *15*(22), 13,041–13,057. https://doi.org/10.5194/acp-15-13041-2015

Tummon, F., Solmon, F., Liousse, C., & Tadross, M. (2010). Simulation of the direct and semidirect aerosol effects on the southern Africa regional climate during the biomass burning season. *Journal of Geophysical Research*, *115*, D19206. https://doi.org/10.1029/2009JD013738

Urbanski, S. P. (2013). Combustion efficiency and emission factors for wildfire-season fires in mixed conifer forests of the northern Rocky Mountains, US. *Atmospheric Chemistry and Physics*, *13*(14), 7241–7262. https://doi.org/10.5194/acp-13-7241-2013

Van Damme, M., Whitburn, S., Clarisse, L., Clerbaux, C., Hurtmans, D., & Coheur, P. F. (2017). Version 2 of the IASI NH_3 neural network retrieval algorithm: Near-real-time and reanalysed datasets. *Atmospheric Measurement Techniques*, *10*(12), 4905–4914. https://doi.org/10.5194/amt-10-4905-2017

van der Werf, G. R., J. T. Randerson, L. Giglio, G. J. Collatz, P. S. Kasibhatla, and A. F. Arellano Jr (2006), Interannual variability in global biomass burning emissions from 1997 to 2004, *Atmospheric Chemistry and Physics*, *6*(11), 3423–3441. https://doi.org/10.5194/acp-6-3423-2006.

van der Werf, G. R., Randerson, J. T., Giglio, L., van Leeuwen, T. T., Chen, Y., Rogers, B. M., Mu, M., et al. (2017). Global fire emissions estimates during 1997–2016. *Earth System Science Data*, *9*(2), 697–720. https://doi.org/10.5194/essd-9-697-2017

van Leeuwen, T. T., Peters, W., Krol, M. C., & van der Werf, G. R. (2013). Dynamic biomass burning emission factors and their impact on atmospheric CO mixing ratios. *Journal of Geophysical Research: Atmospheres*, *118*, 6797–6815. https://doi.org/10.1002/jgrd.50478

Ward, D. E., Hao, W. M., Susott, R. A., Babbitt, R. E., Shea, R. W., Kauffman, J. B., & Justice, C. O. (1996). Effect of fuel composition on combustion efficiency and emission factors for African savanna ecosystems. *Journal of Geophysical Research*, *101*(D19), 23,569–23,576. https://doi.org/10.1029/95JD02595

Whitburn, S., Van Damme, M., Kaiser, J. W., van der Werf, G. R., Turquety, S., Hurtmans, D., Clarisse, L., et al. (2015). Ammonia emissions in tropical biomass burning regions: Comparison between satellite-derived emissions and bottom-up fire inventories. *Atmospheric Environment*, *121*, 42–54. https://doi.org/10.1016/j.atmosenv.2015.03.015

Wooster, M. J., Freeborn, P. H., Archibald, S., Oppenheimer, C., Roberts, G. J., Smith, T. E. L., Govender, N., et al. (2011). Field determination of biomass burning emission ratios and factors via open-path FTIR spectroscopy and fire radiative power assessment: Headfire, backfire and

residual smouldering combustion in African savannahs. *Atmospheric Chemistry and Physics*, *11*(22), 11,591–11,615. https://doi.org/10.5194/acp-11-11591-2011

Wooster, M. J., Roberts, G., Perry, G. L. W., & Kaufman, Y. J. (2005). Retrieval of biomass combustion rates and totals from fire radiative power observations: FRP derivation and calibration relationships between biomass consumption and fire radiative energy release. *Journal of Geophysical Research*, *110*, D24311. https://doi.org/10.1029/2005JD006318

Yin, Y., Chevallier, F., Ciais, P., Broquet, G., Fortems-Cheiney, A., Pison, I., & Saunois, M. (2015). Decadal trends in global CO emissions as seen by MOPITT. *Atmospheric Chemistry and Physics*, *15*(23), 13,433–13,451. https://doi.org/10.5194/acp-15-13433-2015

Yin, Y., Ciais, P., Chevallier, F., van der Werf, G. R., Fanin, T., Broquet, G., Boesch, H., et al. (2016). Variability of fire carbon emissions in equatorial Asia and its nonlinear sensitivity to El Niño. *Geophysical Research Letters*, *43*, 10,472–10,479. https://doi.org/10.1002/2016GL070971

Yokelson, R. J., Bertschi, I. T., Christian, T. J., Hobbs, P. V., Ward, D. E., & Hao, W. M. (2003). Trace gas measurements in nascent, aged, and cloud-processed smoke from African savanna fires by airborne Fourier transform infrared spectroscopy (AFTIR). *Journal of Geophysical Research*, *108*(D13), 8478. https://doi.org/10.1029/2002JD002322

Yokelson, R. J., Burling, I. R., Urbanski, S. P., Atlas, E. L., Adachi, K., Buseck, P. R., Wiedinmyer, C., et al. (2011). Trace gas and particle emissions from open biomass burning in Mexico. *Atmospheric Chemistry and Physics*, *11*(14), 6787–6808. https://doi.org/10.5194/acp-11-6787-2011

Zheng, B., Chevallier, F., Ciais, P., Yin, Y., Deeter, M., Worden, H., Wang, Y. L., et al. (2018). Rapid decline in carbon monoxide emissions and export from East Asia between years 2005 and 2016. *Environmental Research Letters*, *13*(4), 044007. https://doi.org/10.1088/1748-9326/aab2b3